applied sciences

MDPI

Article

Adaptive Robust Fuzzy Impedance Control of an Electro-Hydraulic Actuator

Mingjie Li [1,2,*] and Qiang Zhang [3]

[1] School of Oceanography, Shanghai Jiao Tong University, Shanghai 200030, China
[2] State Key Laboratory of Fluid Power and Mechatronic Systems, Zhejiang University, Hangzhou 310027, China
[3] Hangzhou Doubltech Electro-Hydraulic Engineering Co., Ltd., Hangzhou 310052, China
* Correspondence: mjlee@zju.edu.cn

Abstract: This paper concentrates on both velocity and force control of a single-rod electro-hydraulic actuator in the presence of parameter uncertainties and uncertain nonlinearities. Both velocity control and force control are required in some cases. Impedance control and adaptive robust control are synthesized to deal with this problem. In this paper, the primary goal is velocity control while the contact force is kept in an acceptable range. To keep proper contact force with environment or workpieces, impedance control is adopted to regulate the dynamic relationship between velocity and force. Fuzzy logic is used to adjust the parameters of impedance rules to improve control performance. The velocity command of adaptive robust velocity control is determined by impedance control based on fuzzy logic. Parameter uncertainties and uncertain nonlinearities can be compensated through adaptive robust velocity control, which leads to accurate velocity tracking. The stability of the overall system was analyzed. Comparative experiments verified that the proposed control strategy has both high-accuracy velocity tracking and force regulation performance.

Keywords: adaptive robust control; fuzzy logic; impedance control; electro-hydraulic actuator

Citation: Li, M.; Zhang, Q. Adaptive Robust Fuzzy Impedance Control of an Electro-Hydraulic Actuator. *Appl. Sci.* **2022**, *12*, 9575. https://doi.org/10.3390/app12199575

Academic Editor: Dimitrios Zografopoulos

Received: 1 September 2022
Accepted: 21 September 2022
Published: 23 September 2022

1. Introduction

Electro-hydraulic systems play an important role in construction vehicles, industrial applications, and underwater operations. Accurate velocity control is necessary, e.g., hydraulic elevators [1,2]. Accurate force control is also required, e.g., load simulators [3,4]. Both velocity and force control are required in robot manipulators [5–8], underwater manipulators [9,10] and tunnel boring machines [11,12]. It is necessary to keep an expected dynamic balance between the motion of the actuator and the contact force with the environment or workpieces.

Hogan [13–15] developed impedance control to deal with the dynamics between the actuator and the environment. Impedance control adjusts the dynamic relationship between the position and force of the end effector as a mass-damper-spring system. After this, many researchers paid attention to impedance control. Jamwal et al. [16] developed an impedance control strategy for a lightweight intrinsically compliant parallel ankle rehabilitation robot powered by pneumatic muscle actuators. Hyun et al. [17] implemented proprioceptive impedance control in the MIT Cheetah. Zhang et al. [18] proposed an adaptive impedance control for underwater manipulator teleoperation. Michel et al. [19] presented adaptive impedance control for robotic teleoperation of contact tasks. Hu and Cao [20] proposed a control strategy combining an adaptive variable impedance tracking controller for the slabstone force/position control. Zhao et al. [21] proposed learning algorithms to find the optimal impedance control of human−robot interactions.

Because of the strong parameter uncertainties and uncertain nonlinearities in electro-hydraulic systems, many control algorithms have been employed to obtain high-accuracy motion control. Feedback linearization [22] cancels the known nonlinear terms but cannot

deal with system uncertainties. Adaptive control (AC) [23,24] improves the control system's dynamic performance and static precision. Parameter drift and even instability are the disadvantages of AC when encountering disturbances or measurement noise. Sliding mode control (SMC) [25,26] can compensate system uncertainties and external disturbances, but high frequency modes may be excited and degrade system performance. Yao put forward a control strategy called adaptive robust control (ARC) [27–31], which synthesized AC and SMC effectively. Parameter estimation with smooth limitation can be adopted in ARC to handle parameter drift and system instability, and the chattering problem can be solved in ARC through employing continuous processing of the control input.

A disturbance observer is another way to achieve better motion tracking performance. Since disturbance is always impossible to measure directly in practice, a disturbance observer is an effective strategy to estimate disturbance and cancel its influence. Chen [32] developed a nonlinear disturbance observer to attenuate the disturbance generated by an exogenous system. Guo et al. [33], Li et al. [34], Wei et al. [35], Zhang et al. [36], Shi et al. [37], and Li et al. [38] developed an extended disturbance observer to estimate both external disturbances and uncertain parameters. State estimation errors and tacking errors are both employed to drive the extended disturbance observer, whose effectiveness has been verified in different kinds of electro-hydraulic systems.

Fuzzy control [39–41] is commonly used and does not require a precise system model. Shibata et al. [42] used fuzzy logic-based impedance control to realize force control. Xu and Fang [43] integrated fuzzy logic and neural networks into impedance control to improve performance of the controller. Thus, fuzzy logic could be employed to regulate parameters of impedance rules, which helps to obtain a better performance in different environmental stiffnesses [44].

The current control strategies for hydraulic systems only focus on impedance control or motion control. The two control schemes could be synthesized to improve the control performance of hydraulic systems. Therefore, an adaptive robust fuzzy impedance control (ARFIC) strategy was developed in our research that combines ARC and fuzzy impedance control. ARFIC can not only compensate the parameter uncertainties and uncertain nonlinearities, but also adjust the dynamic behavior between velocity and force. Fuzzy impedance control determines the velocity command. If the contact force lies in the regular range, the velocity command does not change, and high-accuracy velocity tracking performance can be realized. If the contact force exceeds the regular range, the contact force is regulated to an acceptable range by adjusting the velocity command, and an expected dynamic behavior between velocity and force is maintained.

This article is organized as follow. In Section 2, a detailed nonlinear mathematic model of the electro-hydraulic actuator is derived. In Section 3, a fuzzy impedance algorithm is described to regulate output force and velocity. In Section 4, a nonlinear velocity controller based on adaptive robust control and backstepping is designed. In Section 5, the overall control system stability is analyzed. In Section 6, experiments are described to validate the effectiveness of the proposed control strategy. Finally, conclusions are drawn in Section 7.

2. System Modeling

Figure 1 shows a schematic diagram of the electro-hydraulic system under study. The drive cylinder and load cylinder are both controlled by servo valves. The control target is making the controlled mass track a desired velocity trajectory if the load force is within the regular range. Nevertheless, regulation based on the impedance rule is activated to maintain an acceptable output force if the load force exceeds the regular range.

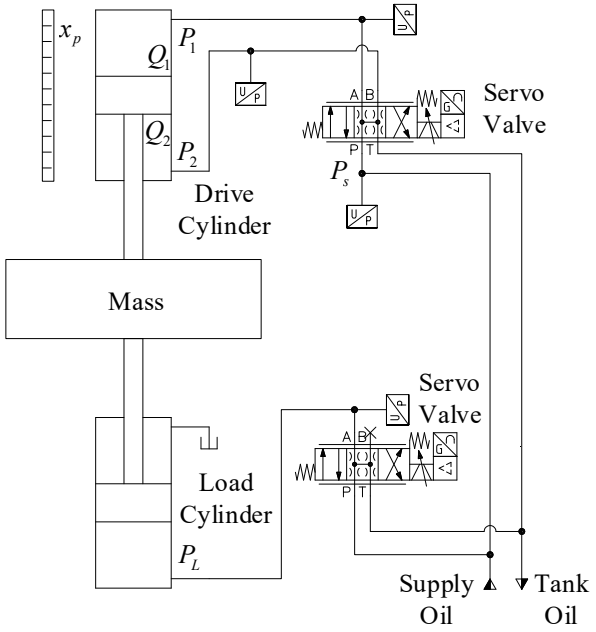

Figure 1. Schematic diagram of the electro-hydraulic system.

As shown in Figure 1, the drive cylinder, load cylinder and mass are combined together as a lumped mass m. Thus, the dynamics of the lumped mass is given by

$$m\ddot{x}_p = P_1A_1 - P_2A_2 - b\dot{x}_p - F_L + G - F_{fc} + f \tag{1}$$

where x_p is the displacement of the load mass, P_1 and P_2 are the pressures of the forward and return chamber of the drive cylinder, A_1 and A_2 are the ram areas of the chambers respectively, b is the damping coefficient, F_L is the load force that is caused by the load cylinder ($F_L = P_LA_3$, P_L is the pressure of load cylinder, A_3 is the corresponding area), G is the gravity of the lumped mass, $F_{fc}(F_{fc}(\dot{x}_p) = F_{fc0}\tanh(\eta\dot{x}_p))$ is the Coulomb friction and f is the lumped uncertain nonlinearities.

Neglecting external leakage, pressure dynamics in the chambers of the drive cylinder are written as

$$\begin{aligned}\dot{P}_1 &= \tfrac{\beta_e}{V_{01}+A_1x_p}\left[Q_1 - A_1\dot{x}_p - C_t(P_1 - P_2)\right]\\ \dot{P}_2 &= \tfrac{\beta_e}{V_{02}-A_2x_p}\left[-Q_2 + A_2\dot{x}_p + C_t(P_1 - P_2)\right]\end{aligned} \tag{2}$$

where V_{01} and V_{02} are the initial volumes of the two chambers in the drive cylinder, β_e is the hydraulic fluid bulk modulus, C_t is the internal leakage coefficient due to pressure of the drive cylinder, and Q_1 and Q_2 are the flow rate of the forward and return chambers, respectively.

The flow rate of the drive cylinder chambers can be expressed as

$$\begin{aligned}Q_1 &= k_qx_v\left[s_g(x_v)\sqrt{P_s - P_1} + s_g(-x_v)\sqrt{P_1 - P_t}\right]\\ Q_2 &= k_qx_v\left[s_g(x_v)\sqrt{P_2 - P_t} + s_g(-x_v)\sqrt{P_s - P_2}\right]\end{aligned} \tag{3}$$

where k_q and x_v are the flow gain coefficient and spool displacement of the servo valve, respectively, P_s is the supply pressure, P_t is the tank pressure, and $s_g(\Delta)$ is defined as

$$s_g(\Delta) = \begin{cases}1, \text{ if } \Delta \geq 0\\ 0, \text{ if } \Delta < 0\end{cases} \tag{4}$$

Since a high response servo valve is applied in the system, the dynamics of the servo valve can be neglected. Therefore, it is assumed that $x_v = k_xu$, where k_x is the gain of servo valve spool and u is the control input voltage. Define $k_{qx} = k_qk_x$.

The state variables are defined as $\mathrm{x} = [x_1, x_2, x_3, x_4]^{\mathrm{T}} = [x_p, \dot{x}_p, P_1, P_2]^{\mathrm{T}}$ and combining (1) to (4), the dynamics of the system in state space form can be expressed as

$$\begin{cases} \dot{x}_1 = x_2 \\ \dot{x}_2 = \frac{1}{m}\left[A_1 x_3 - A_2 x_4 - b x_2 - F_L + G - F_{fc}\right] + d \\ \dot{x}_3 = \beta_e h_1(x_1)\left[-A_1 x_2 - C_t(x_3 - x_4) + k_{qx} u g_1(x_3, u)\right] \\ \dot{x}_4 = \beta_e h_2(x_1)\left[A_2 x_2 + C_t(x_3 - x_4) - k_{qx} u g_2(x_4, u)\right] \end{cases} \tag{5}$$

were

$$\begin{aligned} d &= \tfrac{f}{m} \\ h_1(x) &= \tfrac{1}{V_{01} + A_1 x_1} \\ h_2(x) &= \tfrac{1}{V_{02} - A_2 x_1} \\ g_1(x_3, u) &= s_g(u)\sqrt{P_s - x_3} + s_g(-u)\sqrt{x_3 - P_t} \\ g_2(x_4, u) &= s_g(u)\sqrt{x_4 - P_t} + s_g(-u)\sqrt{P_s - x_4} \end{aligned} \tag{6}$$

A new state variable is introduced as $\overline{x}_3 = x_3 - \alpha x_4$, where $\alpha = A_2/A_1$. Therefore, the system (5) can be dealt with using the backstepping method. Thus, the dynamics of the overall system is transformed into

$$\begin{cases} \dot{x}_1 = x_2 \\ \dot{x}_2 = \frac{1}{m}\left[A_1 \overline{x}_3 - b x_2 - F_L + G - F_{fc}\right] + d \\ \dot{\overline{x}}_3 = \beta_e\left[-f_1 x_2 - f_2 C_t(x_3 - x_4) + k_{qx} f_3 u\right] \end{cases} \tag{7}$$

where

$$\begin{aligned} f_1(x_1) &= h_1(x_1) A_1 + \alpha h_2(x_1) A_2 \\ f_2(x_1) &= h_1(x_1) + \alpha h_2(x_1) \\ f_3(x_1, x_3, x_4, u) &= h_1(x_1) g_1(x_3, u) + \alpha h_2(x_1) g_2(x_4, u) \end{aligned} \tag{8}$$

The following assumption is made before the controller design.

Assumption 1. *The desired velocity trajectory $\dot{x}_d$, and their derivatives $\ddot{x}_d$,$\dddot{x}_d$ are bounded.*

3. Fuzzy Impedance Control

From Figure 1, load force F_L is positively correlated with the drive velocity, which should be kept in a regular range to protect the environment or workpieces. The desired dynamic relationship between velocity and force can be acquired through fuzzy impedance control. Define a first-order impedance rule

$$m_c \ddot{e}_x + b_c \dot{e}_x = e_F \tag{9}$$

where m_c and b_c are the desired mass and damping coefficient, respectively, $e_F = F_L - F_{Ld}$ is the force deviation, F_{Ld} is the desired load force, $\dot{e}_x = \dot{x}_d - \dot{x}$ is the velocity correction, and $\ddot{e}_x$ is its derivative.

A number of impedance rules are required to obtain a better dynamic relationship between velocity and force, due to the variation of velocity command and load force requirement. Therefore, fuzzy logic was adopted to adjust parameters of impedance rules. The parameters were predetermined based on the velocity command and load force requirement.

The fuzzy impedance controller was designed based on Mamdani-type fuzzy inference engine and center of gravity defuzzification. The input and output membership functions are defined as Figures 2 and 3 respectively. Five membership functions are used for input variables V_c and F_c, named as LS, S, M, B, LB in a range of [0, 1], whereas seven membership

functions are used for output variables M and B, named as LS, MS, S, M, B, MB, LB in a range of [0, 1]. The following are the scaling functions

$$\begin{aligned} V_c &= \tfrac{1}{2} + \tfrac{1}{v_{\max} - v_{\min}} \left(v_c - \tfrac{v_{\max} + v_{\min}}{2} \right) \\ F_c &= \tfrac{1}{2} + \tfrac{1}{F_{Ln\max} - F_{Ln\min}} \left(F_{Ln} - \tfrac{F_{Ln\max} + F_{Ln\min}}{2} \right) \\ m_c &= (m_{c\max} - m_{c\min}) \times M + m_{c\min} \\ b_c &= (b_{c\max} - b_{c\min}) \times B + b_{c\min} \end{aligned} \tag{10}$$

where $v_c = \dot{x}_d$ is the velocity command, $v_{\max}$ and $v_{\min}$ are its maximum and minimum values; F_{Ln} is the nominal load force, and $F_{Ln\max}$ and $F_{Ln\min}$ are its maximum and minimum values. The nominal load force can be measured in advance. It is the force of the load cylinder when it moves at a desired velocity with a normal load. $m_{c\max}$ and $m_{c\min}$ are the maximum and minimum values of desired mass, and $b_{c\max}$ and $b_{c\min}$ are the maximum and minimum values of desired damping coefficient.

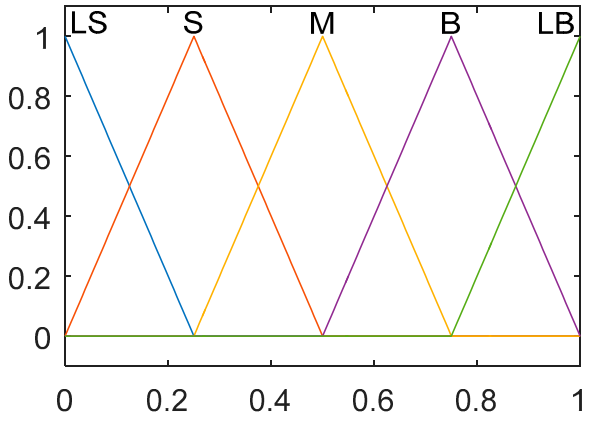

Figure 2. Membership functions for inputs.

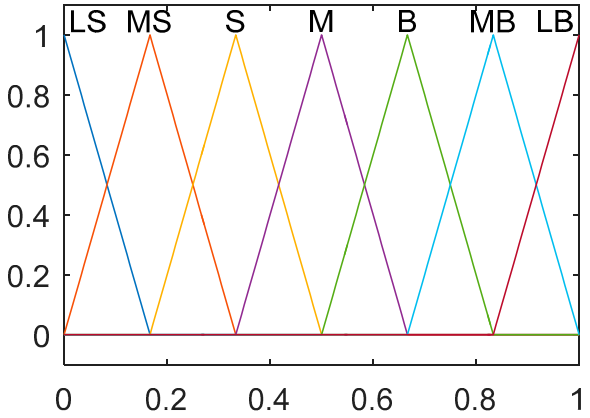

Figure 3. Membership functions for outputs.

Tables 1 and 2 show the fuzzy rules, velocity command V_c and nominal load force F_c are the input variables, whereas desired mass M and desired damping coefficient B are the output variables. The goal of fuzzy impedance control is to adjust the load force to an acceptable range and provide an expected dynamic response between velocity and load force. According to the load cylinder in the system, a larger velocity leads to a larger load force that requires a smaller m_c to improve the dynamics, and a larger b_c to ease the restriction of the load force, respectively. A larger nominal load force also demands a smaller m_c and a larger b_c, because the system is much more vulnerable to disturbances, which means a small change of velocity will result in a larger change of load force.

Table 1. Fuzzy rules of desired mass M.

M		V_c				
		LS	**S**	**M**	**B**	**LB**
F_c	LS	LB	LB	MB	B	M
	S	LB	MB	B	M	S
	M	MB	B	M	S	MS
	B	B	M	S	MS	LS
	LB	M	S	MS	LS	LS

Table 2. Fuzzy rules of desired damping coefficient B.

B		V_c				
		LS	**S**	**M**	**B**	**LB**
F_c	LS	LS	LS	MS	S	M
	S	LS	MS	S	M	B
	M	MS	S	M	B	MB
	B	S	M	B	MB	LB
	LB	M	B	MB	LB	LB

Considering fuzzy impedance control in the control process, the desired velocity trajectory turns into $\dot{x}_s = \dot{x}_d - \dot{\bar{e}}_x$, and the derivatives become $\ddot{x}_s = \ddot{x}_d - \ddot{\bar{e}}_x$, $\dddot{x}_s = \dddot{x}_d - \dddot{\bar{e}}_x$. $\dot{\bar{e}}_x$, $\ddot{\bar{e}}_x$ and $\dddot{\bar{e}}_x$ are the computation results of (9), which are different from $\dot{e}_x$, $\ddot{e}_x$ and $\dddot{e}_x$.

Assumption 2. *Based on Assumption 1 and the first-order impedance rule, $\dot{x}_s$, $\ddot{x}_s$, $\dddot{x}_s$ are assumed to be bounded.*

4. Adaptive Robust Velocity Control

4.1. Model Analysis

Parameter uncertainties are unavoidable in the electro-hydraulic system, such as the variations of m, b, F_{fc}, β_e, k_q, k_x and so on. For simplicity, only the prime parameters, m, β_e and d_n (the nominal value of system uncertain nonlinearity d, $d = d_n + \widetilde{d}$) are taken into parameters adaption.

Define the unknown parameters set as $\theta = \begin{bmatrix}\theta_1 & \theta_2 & \theta_3\end{bmatrix}^T = \begin{bmatrix}1/m & d_n & \beta_e\end{bmatrix}^T$. Thus, the system dynamics (7) is transformed to

$$\begin{cases} \dot{x}_1 = x_2 \\ \dot{x}_2 = \theta_1\left[A_1\overline{x}_3 - bx_2 - F_L + G - F_{fc}\right] + \theta_2 + \widetilde{d} \\ \dot{\overline{x}}_3 = \theta_3\left[-f_1x_2 - f_2C_t(x_3 - x_4) + k_{qx}f_3u\right] \end{cases} \tag{11}$$

In practical applications, the extents of parameters and uncertain nonlinearity are known. So, we made the following assumption.

Assumption 3. *The parameter uncertainties and uncertain nonlinearity are bounded as*

$$\begin{aligned} &\theta \in \Omega_\theta \triangleq \{\theta : \theta_{\min} \le \theta \le \theta_{\max}\} \\ &\left|\widetilde{d}\right| \le \delta \end{aligned} \tag{12}$$

In (12), the operation '$\le$' is performed in terms of the corresponding elements of the vectors. In practice,$\theta_{\min} = \begin{bmatrix}\theta_{1\min} & \theta_{2\min} & \theta_{3\min}\end{bmatrix}^T$, $\theta_{\max} = \begin{bmatrix}\theta_{1\max} & \theta_{2\max} & \theta_{3\max}\end{bmatrix}^T$, δ are all known, and $\theta_{1\min} > 0$, $\theta_{3\min} > 0$.

4.2. Projection Mapping and Parameter Adaptation

Define $\hat{\theta}$ as the estimation of θ and estimation error as $\widetilde{\theta} = \theta - \hat{\theta}$. A discontinuous projection [45] is defined as

$$\mathrm{Proj}_{\hat{\theta}_i} = \begin{cases} 0, \ \hat{\theta}_i = \theta_{i\max} \text{ and } \bullet_i > 0 \\ 0, \ \hat{\theta}_i = \theta_{i\min} \text{ and } \bullet_i < 0 \\ \bullet_i, \text{otherwise} \end{cases} \tag{13}$$

where $i = 1, 2, 3$, '$\bullet_i$' is the ith element of the vector '$\bullet$'. Under this projection, an adaption law [45] is given

$$\dot{\hat{\theta}} = \mathrm{Proj}_{\hat{\theta}}(\Gamma\tau), \text{ with } \theta_{\min} \le \hat{\theta}(0) \le \theta_{\max} \tag{14}$$

where $\Gamma = diag\{ \ \Gamma_1 \quad \Gamma_2 \quad \Gamma_3 \ \}$ is a symmetric positive definite adaption rate matrix, and τ is an adaption function to guarantee

$$\begin{cases} \hat{\theta} \in \Omega_{\hat{\theta}} \triangleq \{\hat{\theta} : \theta_{\min} \le \hat{\theta} \le \theta_{\max}\} \\ \widetilde{\theta}^T \left[\Gamma^{-1}\mathrm{Proj}_{\hat{\theta}}(\Gamma\tau) - \tau\right] \le 0 \end{cases} \tag{15}$$

4.3. Velocity Control Design

The velocity control consists of an outer-loop velocity control and an inner-loop pressure control. According to the recursive backstepping technique, a velocity controller can be designed.

Step 1:

The velocity tracking error is defined as $z_1 = x_2 - \dot{x}_s$. Then, a sliding surface z_2 can be defined as

$$z_2 = z_1 + k_1 \int z_1 dt \tag{16}$$

where k_1 is a positive constant. Since making z_1 small or converge to zero is same as making z_2 small or converge to zero, the rest of the controller design concentrates on making z_2 as small as possible. Differentiating (16) and noting (11) based on Assumption 2, yielding

$$\dot{z}_2 = \theta_1 \left[A_1 \overline{x}_3 - b x_2 - F_L + G - F_{fc}\right] + \theta_2 + \widetilde{d} - \dot{x}_{2eq} \tag{17}$$

where $\dot{x}_{2eq} = \ddot{x}_s - k_1(x_2 - \dot{x}_s)$.

A virtual control input α_2 for $\overline{x}_3$ is designed as

$$\begin{aligned} &\alpha_2 = \alpha_{2a} + \alpha_{2s} \\ &\alpha_{2a} = \tfrac{1}{A_1}\left[\left(b x_2 + F_L - G + F_{fc}\right) + \hat{\theta}_1(\dot{x}_{2eq} - \hat{\theta}_2)\right] \\ &\alpha_{2s} = \alpha_{2s1} + \alpha_{2s2} \\ &\alpha_{2s1} = -k_{2s1} z_2, \ k_{2s1} \ge \tfrac{1}{\theta_{1\min} A_1}\left(\left\|C_{\phi_2}\Gamma\phi_2\right\|^2 + k_2\right) \\ &\tau_2 = w_2 \phi_2 z_2, \ w_2 > 0 \end{aligned} \tag{18}$$

where C_{ϕ_2} is a positive definite constant diagonal matrix, and α_{2s2} is a robust control function, which will be designed later. k_2 and w_2 are positive constants, k_{2s1} is the positive feedback coefficient in the outer velocity control loop. ϕ_2 is defined as

$$\phi_2 = \left[\ A_1\alpha_{2a} - b x_2 - F_L + G - F_{fc} \ 1 \ 0 \ \right]^T \tag{19}$$

α_{2a} is a model compensation through online parameter adaption, α_{2s} is a robust control law, of which α_{2s2} is a function satisfying the following conditions [45]

$$\begin{aligned} &\text{i } z_2\left[\theta_1\alpha_{2s2} - \widetilde{\theta}^T\phi_2 + \widetilde{d}\right] \le \varepsilon_2 \\ &\text{ii } z_2\alpha_{2s2} \le 0 \end{aligned} \tag{20}$$

where ε_2 is a positive constant that can arbitrarily be small.

Define a following Lyapunov function

$$V_2 = \frac{1}{2}w_2 z_2^2 \tag{21}$$

Let $z_3 = \overline{x}_3 - \alpha_2$ represent the tracking error of the inner pressure control loop, and taking (17)–(19) into account, the time derivative of V_2 is expressed as

$$\dot{V}_2 = w_2\theta_1 A_1 z_2 z_3 + w_2 A_1 z_2\left(\theta_1\alpha_{2s2} - \widetilde{\theta}\phi_2 + \widetilde{d}\right) - w_2\theta_1 A_1 k_{2s1} z_2^2 \tag{22}$$

Step 2:

The time derivative of z_3 is expressed as

$$\dot{z}_3 = \theta_3\left[-f_1 x_2 - f_2 C_t(x_3 - x_4) + k_{qx} f_3 u\right] - \dot{\alpha}_{2c} - \dot{\alpha}_{2u} \tag{23}$$

where

$$\begin{aligned} \dot{\alpha}_{2c} &= \tfrac{\partial\alpha_2}{\partial x_1}x_2 + \tfrac{\partial\alpha_2}{\partial x_2}\hat{\dot{x}}_2 + \tfrac{\partial\alpha_2}{\partial t} \\ \dot{\alpha}_{2u} &= \tfrac{\partial\alpha_2}{\partial x_2}\left[-\left(A_1\overline{x}_3 - bx_2 - F_L + G - F_{fc}\right)\widetilde{\theta}_1 - \widetilde{\theta}_2 + \widetilde{d}\right] + \tfrac{\partial\alpha_2}{\partial\hat{\theta}}\dot{\hat{\theta}} \end{aligned} \tag{24}$$

$\dot{\alpha}_{2c}$ is the calculable part of α_2, which will be used in the control function design, $\dot{\alpha}_{2u}$ is the incalculable part which should be handled with robust feedback. $\hat{\dot{x}}_2$ represents the calculable part of $\dot{x}_2$, from (11), $\hat{\dot{x}}_2$ can be expressed as

$$\hat{\dot{x}}_2 = \hat{\theta}_1\left[A_1\overline{x}_3 - bx_2 - F_L + G - F_{fc}\right] + \hat{\theta}_2 \tag{25}$$

The actual control input u needs to be designed to make $\overline{x}_3$ track the virtual control input α_2. Similar as *Step 1*, u is given by

$$\begin{aligned} &u = u_a + u_s \\ &u_a = \tfrac{1}{k_{qx}f_3}\left[f_1 x_2 + f_2 C_t(x_3 - x_4) + \tfrac{\dot{\alpha}_{2c}}{\hat{\theta}_3} - \tfrac{w_2\hat{\theta}_1 A_1 z_2}{w_3\hat{\theta}_3} - \tfrac{\partial\alpha_2}{\partial\hat{\theta}}\mathrm{Proj}_{\hat{\theta}}(\Gamma\tau)\right] \\ &u_s = u_{s1} + u_{s2} \\ &u_{s1} = -\tfrac{k_{3s1}}{k_{qx}f_3}z_3, k_{3s1} \ge \tfrac{1}{\theta_{3\min}}\left(k_3 + \left\|\tfrac{\partial\alpha_2}{\partial\hat{\theta}}C_{\theta_3}\right\|^2 + \left\|C_{\phi_3}\Gamma\phi_3\right\|^2\right) \\ &\tau = \tau_2 + w_3\phi_3 z_3,\ w_3 > 0 \end{aligned} \tag{26}$$

where C_{θ_3} and C_{ϕ_3} are positive definite constant diagonal matrixes, and α_{2s2} is a robust control function designed later. k_3 and w_3 are positive constants, k_{3s1} is the positive feedback coefficient in the inner pressure control loop. ϕ_3 is defined as

$$\phi_3 = \begin{bmatrix} \frac{w_2}{w_3}A_1 z_2 - \frac{\partial\alpha_2}{\partial x_2}\left(A_1\overline{x}_3 - bx_2 - F_L + G - F_{fc}\right) \\ -\frac{\partial\alpha_2}{\partial x_2} \\ k_{qx}f_3 u_a - f_1 x_2 - f_2 C_t(x_3 - x_4) \end{bmatrix} \tag{27}$$

u_a is a model compensation through online parameter adaption, u_s is a robust control law, of which u_{s2} is a function satisfying the following conditions [45]

$$\begin{aligned} &\text{i } z_3\left[\theta_3 k_{qx} f_3 u_{s2} - \widetilde{\theta}^T \phi_3 - \tfrac{\partial \alpha_2}{\partial x_2}\widetilde{d}\right] \le \varepsilon_3 \\ &\text{ii } z_3 u_{s2} \le 0 \end{aligned} \tag{28}$$

where ε_3 is a positive constant which can arbitrarily be small.

Define a following Lyapunov function

$$V_3 = V_2 + \frac{1}{2} w_3 z_3^2 \tag{29}$$

Taking Equations (22)–(24) and (26) into account, the time derivative of V_3 is expressed as

$$\begin{aligned} \dot{V}_3 = \; & w_2 A_1 z_2 \left(\theta_1 \alpha_{2s2} - \widetilde{\theta}\phi_2 + \widetilde{d}\right) - w_2 \theta_1 A_1 k_{2s1} z_2^2 \\ & + w_3 z_3 \left[\theta_3 k_{qx} f_3 u_{s2} - \widetilde{\theta}^T \phi_3 - \tfrac{\partial \alpha_2}{\partial x_2}\widetilde{d}\right] - w_3 \theta_3 k_{3s1} z_3^2 - w_3 z_3 \tfrac{\partial \alpha_2}{\partial \hat{\theta}} \dot{\hat{\theta}} \end{aligned} \tag{30}$$

4.4. Stability of ARC

For simplicity, choosing nonlinear controller gains k_{2s1} and k_{3s1} large enough [45] so that the inequality conditions in (18) and (26) are satisfied for $C_{\theta_j} = diag\left\{c_{\theta_{jl}}\right\}$, $l = 1,2,3, j = 3$ and $C_{\phi_k} = diag\{c_{\phi_{kl}}\}, k = 2,3$ with $c_{\phi_{kl}}^2 \ge \frac{3 w_k w_3}{4 c_{\theta_{3l}}^2}, \forall k, l$, then the control input as (26) with the adaption law (14) guarantees that

$$V_4 \le \exp(-\lambda_V t) V_4(0) + \frac{\varepsilon_V}{\lambda_V}[1 - \exp(-\lambda_V t)] \tag{31}$$

where $\lambda_V = 2\min\{k_2, k_3\}$ and $\varepsilon_V = A_1 w_2 \varepsilon_2 + w_3 \varepsilon_3$.

Proof of (31).

$$\begin{aligned} & \left| w_3 z_3 \tfrac{\partial \alpha_2}{\partial \hat{\theta}} \dot{\hat{\theta}} \right| = \left| \textstyle\sum_{k=2}^{3} w_3 z_3 \tfrac{\partial \alpha_2}{\partial \hat{\theta}} \tfrac{1}{\sqrt{3 w_3}} C_{\theta_3} \sqrt{3 w_3} C_{\theta_3}^{-1} \Gamma \phi_k w_k z_k \right| \\ & \le \textstyle\sum_{k=2}^{3} \left(\tfrac{1}{\sqrt{3}} \sqrt{w_3} |z_3| \left\| C_{\theta_3} \left(\tfrac{\partial \alpha_2}{\partial \hat{\theta}} \right)^T \right\| \right) \left(\sqrt{3 w_3 w_k} \left\| C_{\theta_3}^{-1} \Gamma \phi_k \right\| \sqrt{w_k} |z_k| \right) \\ & \le \textstyle\sum_{k=2}^{3} \left[\tfrac{1}{3} w_3 z_3^2 \left\| C_{\theta_3} \left(\tfrac{\partial \alpha_2}{\partial \hat{\theta}} \right)^T \right\|^2 + \tfrac{3}{4} w_3 w_k \left\| C_{\theta_3}^{-1} \Gamma \phi_k \right\|^2 w_k z_k^2 \right] \\ & \le w_3 \left\| C_{\theta_3} \left(\tfrac{\partial \alpha_2}{\partial \hat{\theta}} \right)^T \right\|^2 z_3^2 + \textstyle\sum_{k=2}^{3} w_k \left(\tfrac{3}{4} w_k w_3 \left\| C_{\theta_3}^{-1} \Gamma \phi_k \right\|^2 \right) z_k^2 \end{aligned} \tag{32}$$

If C_{ϕ_j} and C_{θ_j} satisfy the aforementioned condition, then (32) becomes

$$\left| w_3 z_3 \frac{\partial \alpha_2}{\partial \hat{\theta}} \dot{\hat{\theta}} \right| \le w_3 \left\| C_{\theta_3} \left(\frac{\partial \alpha_2}{\partial \hat{\theta}} \right)^T \right\|^2 z_3^2 + \sum_{k=2}^{3} w_k \left(\left\| C_{\theta_3} \Gamma \phi_k \right\|^2 \right) z_k^2 \tag{33}$$

Thus, considering the formula for k_{2s1} and k_{3s1}, (30) turns into

$$\begin{aligned} \dot{V}_3 \le \; & -w_2 k_2 z_2^2 - w_3 k_3 z_3^2 + w_2 A_1 z_2 \left(\theta_1 \alpha_{2s2} - \widetilde{\theta}\phi_2 + \widetilde{d}\right) \\ & + w_3 z_3 \left[\theta_3 k_{qx} f_3 u_{s2} - \widetilde{\theta}^T \phi_3 - \tfrac{\partial \alpha_2}{\partial x_2}\widetilde{d}\right] \end{aligned} \tag{34}$$

Noting the condition i of Equations (20) and (28) yields

$$\dot{V}_3 \le -w_2 k_2 z_2^2 - w_3 k_3 z_3^2 + A_1 w_2 \varepsilon_2 + w_3 \varepsilon_3 \le -2\lambda_V V_3 + \varepsilon_V \tag{35}$$

which leads to (31).

If, after a finite time, t_0, $\widetilde{d} = 0$, i.e., only exiting parameter uncertainties, apart from results in (31), asymptotic output tracking (i.e., zero final tracking error) can be achieved [45].

This can be proved by defining a new Lyapunov function

$$V = V_3 + \frac{1}{2}\widetilde{\theta}^T \Gamma^{-1} \widetilde{\theta} \tag{36}$$

Assume the unknown parameter vector is constant; thus, $\dot{\widetilde{\theta}} = \dot{\hat{\theta}}$, so the time derivative of V is

$$\dot{V} \leq -\sum_{j=2}^{3} w_j k_j z_j^2 - \widetilde{\theta}^T \tau + \widetilde{\theta}^T \Gamma^{-1} \dot{\hat{\theta}} \leq -\sum_{j=2}^{3} w_j k_j z_j^2 \tag{37}$$

Therefore, the stability of the ARC designed above is proved. □

5. Stability Analysis of the Whole System

As Figure 4 shown, a fuzzy impedance controller and a nonlinear velocity controller are synthesized together in the whole cascade system. The parameters of impedance rules are predetermined. Thus, the impedance system (9) is a time invariant first-order system with positive coefficients. According to the concerned load system, the input e_F is bounded. Therefore, the impedance system is stable based on Routh's stability criterion.

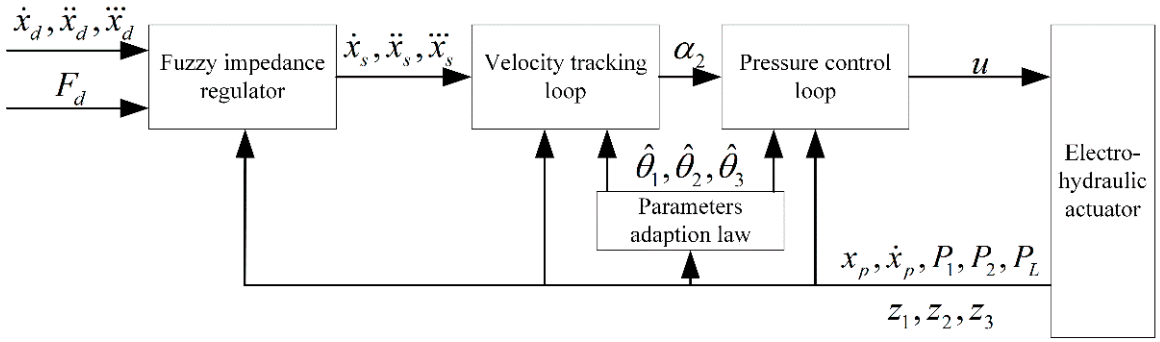

Figure 4. Schematic diagram of the proposed ARFIC control strategy.

Defining a sliding function as

$$s_I = m_c \ddot{e}_x + b_c \dot{e}_x - e_F \tag{38}$$

it can be seen that the sliding function (38) generates the expected impedance behavior (46), when s_I vanishes [46]. The above definitions yield

$$\begin{aligned} s_I &= m_c\left(\ddot{x}_d - \ddot{x}\right) + b_c\left(\dot{x}_d - \dot{x}\right) - e_F \\ &= m_c\left(-\dot{z}_1 + \dddot{e}_x\right) + b_c\left(-z_1 + \ddot{e}_x\right) - e_F \\ &= -\left(m_c \dot{z}_1 + b_c z_1\right) \end{aligned} \tag{39}$$

Since the stability of ARC is already proved, z_1 will converge to zero after a finite time only under parameter uncertainties. To make the force vary smoothly, the response of ARC is designed much faster than the fuzzy impedance controller. Thus, $\ddot{x}_s$ and $\dot{x}_2$ can be finally treated as small enough, since $\dot{x}_d$ is always set as constant and the load is assumed to vary slowly in practice. Then, $\dot{z}_1 = \dot{x}_2 - \ddot{x}_s$ can be considered small enough to make s_I converge to zero. Consequently, impedance performance can be guaranteed under certain conditions.

6. Experimental Results

Experiments were conducted to validate the performance of the proposed ARFIC. The drive cylinder and the load cylinder were both controlled by servo valves. Four pressure sensors were utilized. A position sensor was used to obtain the displacement and velocity of the drive cylinder. A data acquisition card was employed to collect data and output control inputs. The control strategy was implemented in the MATLAB Simulink Realtime environment with a 1 kHz control rate.

Firstly, ARC (without impedance control) was tested. Table 3 lists the parameters of the electro-hydraulic system. Tables 4 and 5 list controller parameters. Figure 5 shows the desired velocity trajectory, $\dot{x}_d = 0.02\sin\left(\frac{\pi}{5}t + \frac{3\pi}{2}\right) + 0.03$ m/s. $u_L = -2$ V is the servo valve command of load cylinder. As Figure 6 shown, the tracking errors of ARC were small. Figure 7 shows the control input and Figure 8 shows the parameter estimations. ARC achieved accurate velocity tracking, because the parameter uncertainties and uncertain nonlinearities could be compensated. The initial values of parameter estimations were defined according to parameter identification when $\dot{x}_d = 0.02$ m/s. However, it cannot be guaranteed that parameter estimations converged to true values because only control errors were used to drive the parameter adaption law, and persistent excitation condition [47] may not be satisfied.

Table 3. Parameters of the electro-hydraulic system.

Symbol	Value	Unit
A_1	5.0265×10^{-3}	m^2
A_2	3.0631×10^{-3}	m^2
b	1×10^5	Ns/m
F_{fc0}	1.2×10^3	N
η	10	
G	1715	N
A_3	3.8485×10^{-3}	m^2
P_s	2.1×10^6	Pa
P_t	0	Pa
C_t	0	m^4/kg
k_{qx}	3.5635×10^{-8}	$m^3/\left(sV\sqrt{Pa}\right)$

Table 4. Nominal Values and bounds of θ_i.

Symbol (Unit)	Nominal Value	$\theta_{i\min}$	$\theta_{i\max}$
$\theta_1(1/kg)$	5.7143×10^{-3}	5×10^{-4}	6×10^{-2}
$\theta_2(N/kg)$	0	-30	30
$\theta_3(Pa)$	7×10^8	7×10^7	7×10^9

Table 5. Parameters of ARC.

Symbol	Value	Symbol	Value
k_1	56	Γ_1	1×10^{-18}
k_{2s1}	1.86×10^7	Γ_2	5×10^{-12}
k_{3s1}	5×10^{-7}	Γ_3	1×10^4

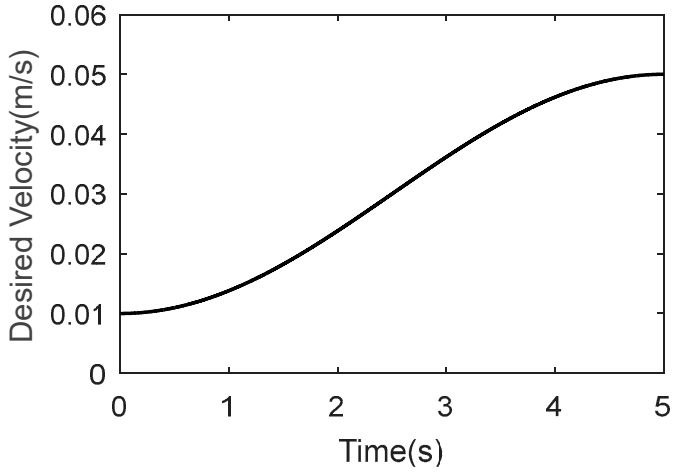

Figure 5. Desired velocity trajectory.

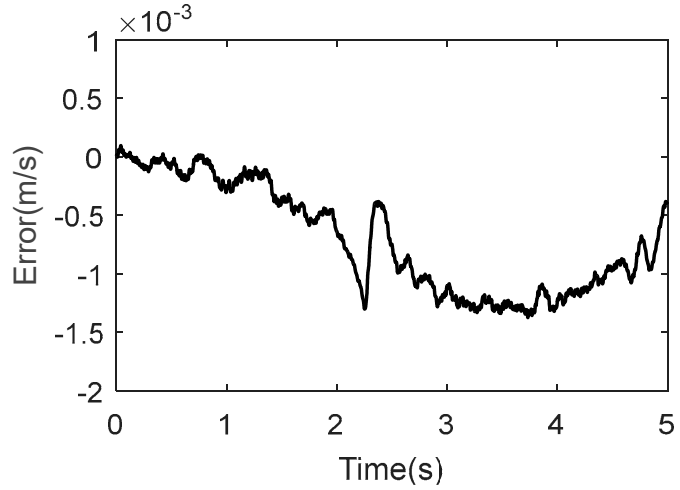

Figure 6. Tracking errors of ARC.

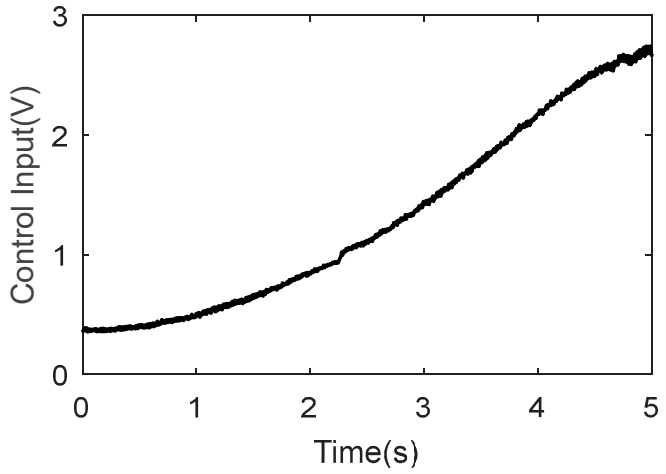

Figure 7. Control input of ARC.

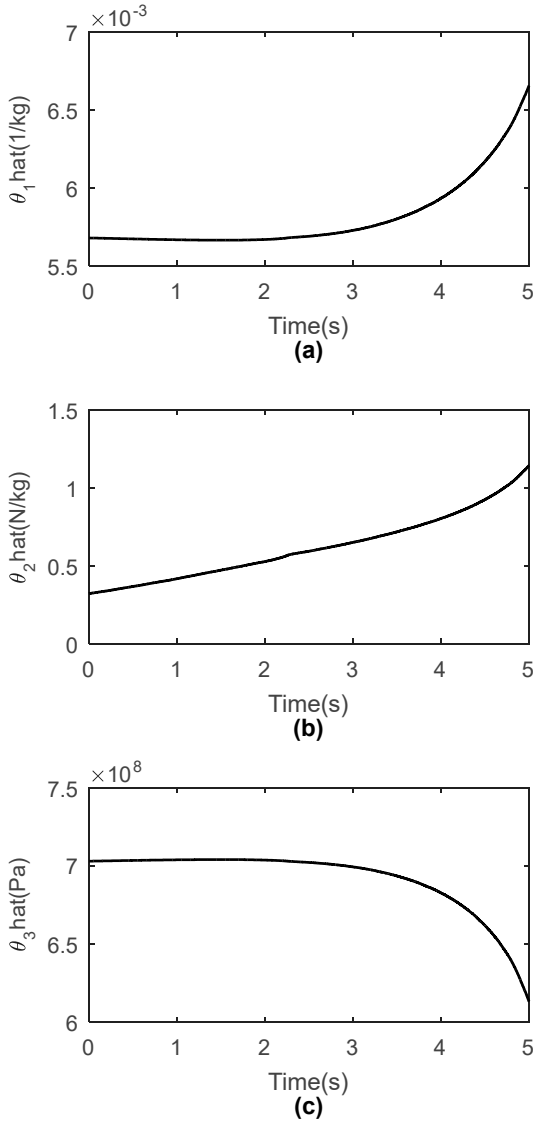

Figure 8. Parameter estimations of ARC: (**a**) estimation of θ_1; (**b**) estimation of θ_2; (**c**) estimation of θ_3.

Next, ARFIC was verified when the velocity command was constant at 0.02 m/s and 0.04 m/s. The parameters of the fuzzy impedance rule were chosen according to Table 6. ARFIC was tested compared with ARC (without impedance control), to validate the effectiveness of fuzzy impedance control. A step-like signal was applied to the servo valve which controls the load cylinder. A pressure sensor was used to measure the load force in experiments.

Table 6. Parameters of the fuzzy impedance rule.

Symbol	Value	Unit
$v_{\max}$	0.05	m/s
$v_{\min}$	0.01	m/s
$F_{Ln\max}$	6×10^4	N
$F_{Ln\min}$	2000	N
$m_{c\max}$	850	Ns^2/m
$m_{c\min}$	350	Ns^2/m
$b_{c\max}$	1×10^6	Ns/m
$b_{c\min}$	1×10^5	Ns/m

As shown in Figure 9a, the velocity command was 0.02 m/s, and the load command changed in a step-wise manner from −1 V to −0.7 V then to −1 V. The regulated velocity commands are shown in Figure 9b, which guaranteed an expected impedance behavior when load command change occurred. A smooth smaller velocity command was produced by fuzzy impedance control in ARFIC. The load force of ARFIC was kept in a close range, as shown in Figure 9d. Tracking errors with respect to unregulated or regulated velocity command are shown in Figure 9c. Both ARFIC and ARC achieved accurate velocity tracking. ARFIC showed a great ability to handle load change through velocity adjustment.

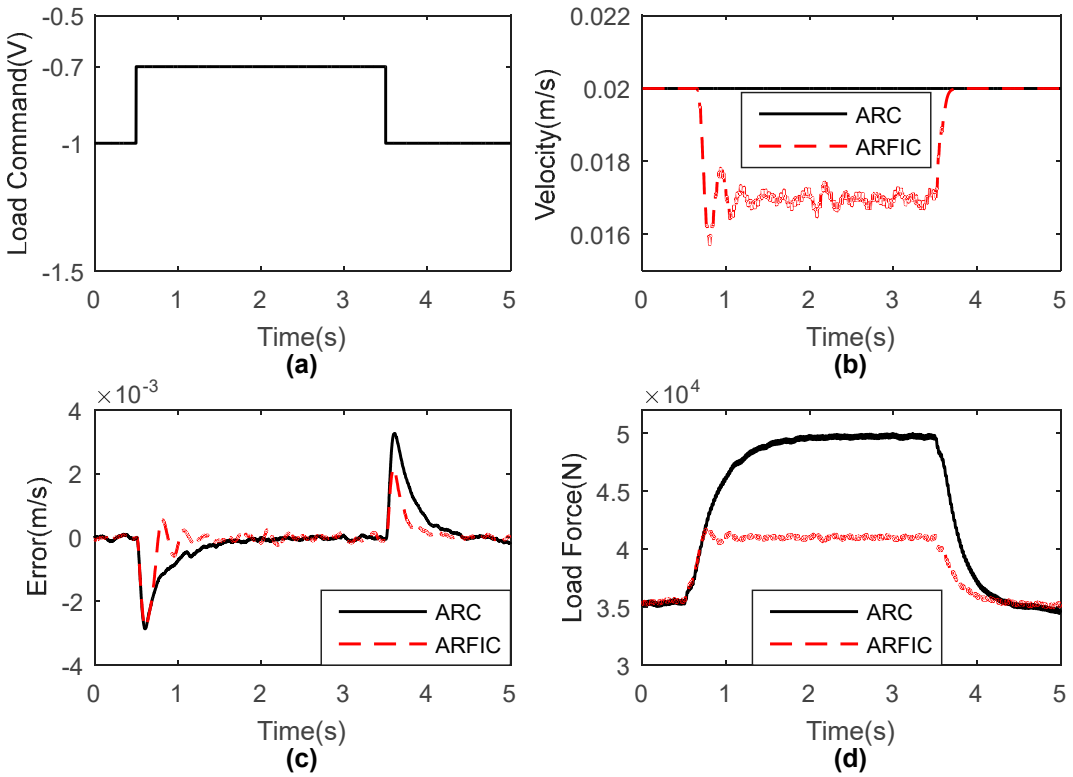

Figure 9. Tracking performance with a 0.02 m/s velocity command and −1 V ∼ −0.7 V ∼ −1 V load command: (**a**) load command; (**b**) velocity commands; (**c**) velocity tracking errors; (**d**) load forces.

Fuzzy impedance control worked when the deviation of load force exceeded 10% of the nominal value in experiments. It can be seen that dynamic balance behavior was achieved with a fuzzy logic-based impedance control. To validate the effectiveness of ARFIC further, some other load and velocity commands were tested. Similarly, in all kinds of cases, ARFIC demonstrated accurate velocity tracking and impedance regulation between velocity and force. The experiment results are shown in Figures 10–12. A smooth regulated velocity command was generated when the load force was beyond the regular range. ARFIC could keep the load force in a close range, comparing with ARC.

Impedance control regulates the load force in a close area which can protect the environment or workpieces. It is quite useful in practice, because motion control has to consider the contact force with the environment or workpieces. ARFIC provides a solution to keep a compromise of velocity control and force control. In ARFIC, contact force is considered as the protection for the system, which should be kept in an acceptable range. Accurate velocity tracking can be achieved, when the contact force is in the regular range, but the velocity command is adjusted, when the contact force exceeds the regular range.

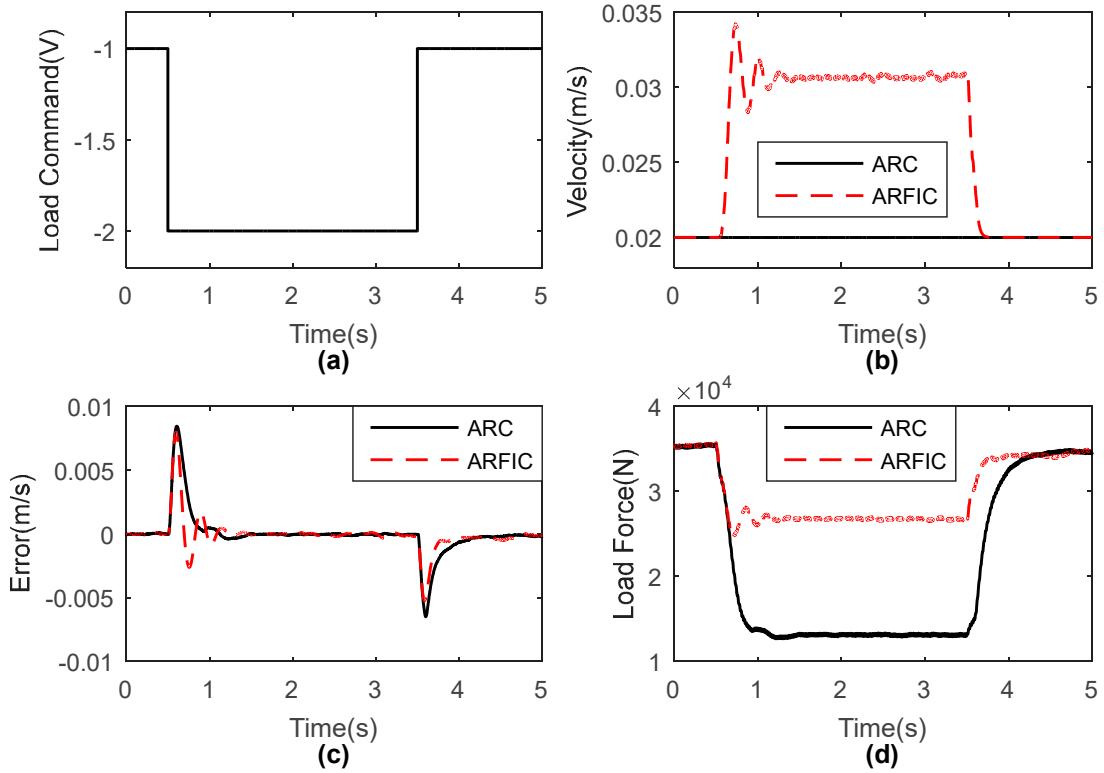

Figure 10. Tracking performance with a 0.02 m/s velocity command and -1 V ~ -2 V ~ -1 V load command: (**a**) load command; (**b**) velocity commands; (**c**) velocity tracking errors; (**d**) load forces.

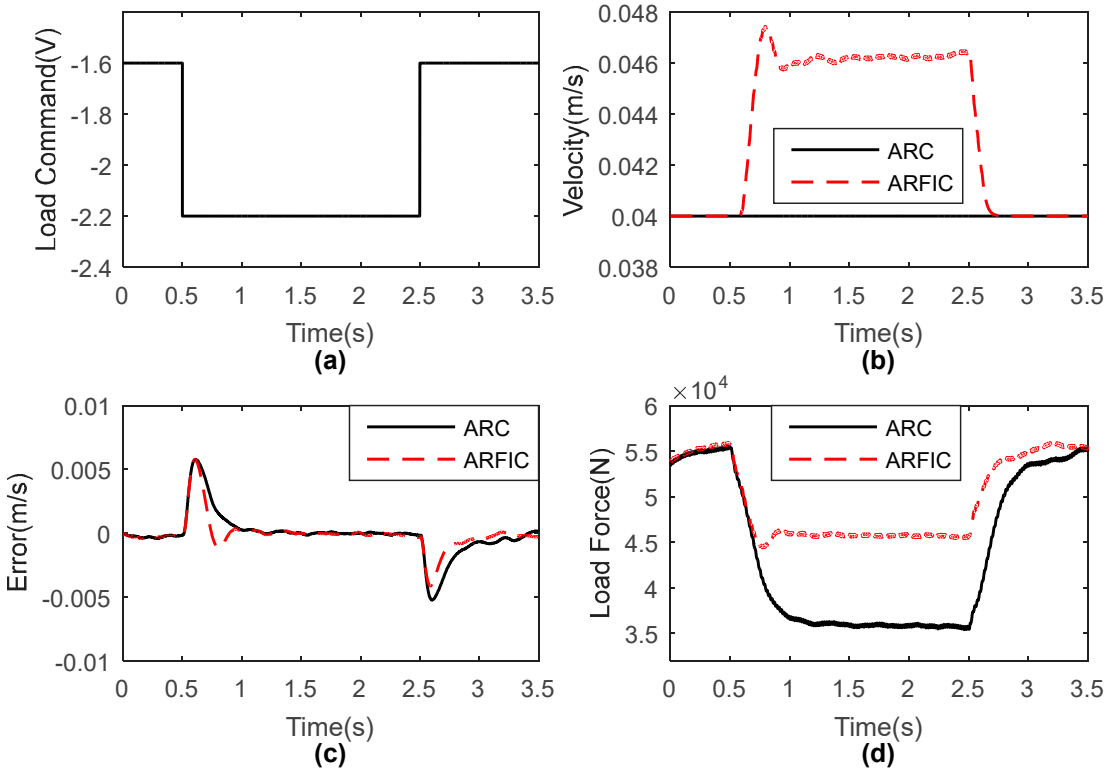

Figure 11. Tracking performance with a 0.04 m/s velocity command and -1.6 V ~ -2.2 V ~ -1.6 V load command: (**a**) load command; (**b**) velocity commands; (**c**) velocity tracking errors; (**d**) load forces.

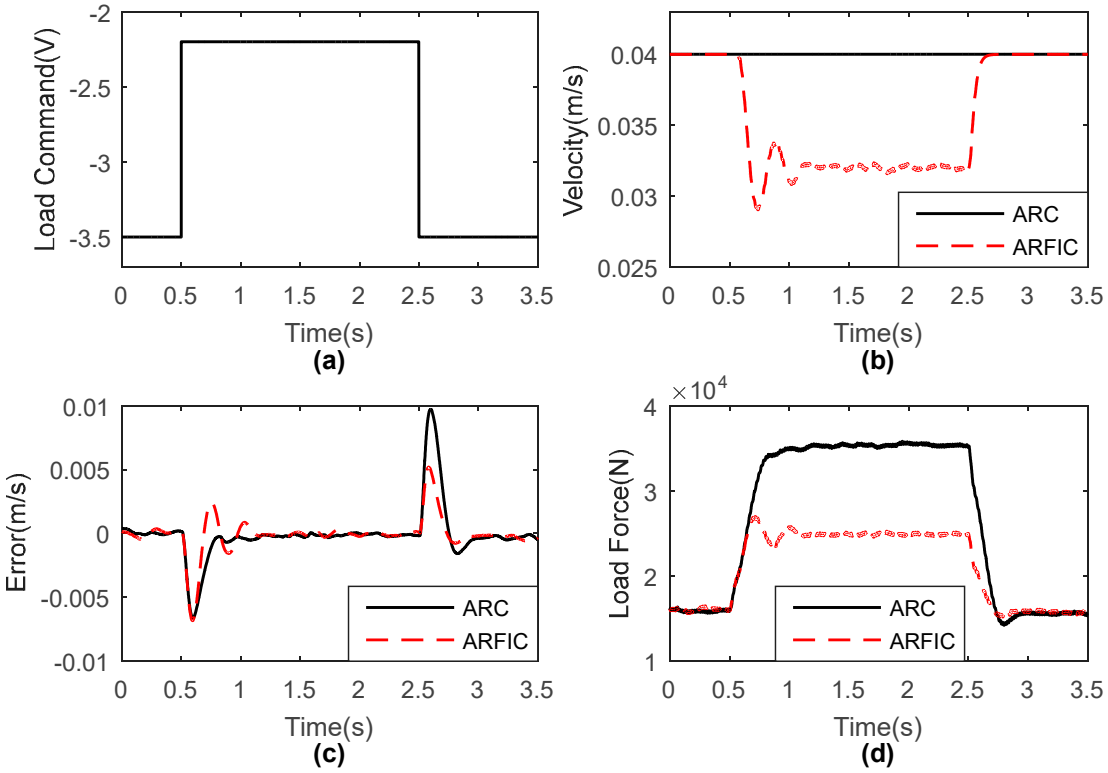

Figure 12. Tracking performance with a 0.04 m/s velocity command and -3.5 V ~ -2.2 V ~ -3.5 V load command: (**a**) load command; (**b**) velocity commands; (**c**) velocity tracking errors; (**d**) load forces.

7. Conclusions

In this research, an adaptive robust controller and an impedance control strategy were developed to handle both velocity and force control for an electro-hydraulic actuator. The developed control strategy has the merits of an adaptive robust controller and impedance controller. Parameter uncertainties and uncertain nonlinearities could be compensated through ARC, which led to high-accuracy velocity tracking. A compromise of velocity control and force control could be acquired through the impedance controller. Fuzzy logic was employed to tune the parameters of the impedance controller to obtain better performance. The velocity command was regulated by the fuzzy impedance controller, which is the control target of ARC. The stability of the whole cascade system was analyzed. In experiments, parameter uncertainties and uncertain nonlinearities were successfully canceled, and high-accuracy velocity tracking and force regulation were also attained, which validated the effectiveness of the ARFIC strategy.

Author Contributions: Conceptualization, M.L.; methodology, M.L. and Q.Z.; formal analysis, M.L.; writing—original draft preparation, M.L.; writing—review and editing, Q.Z. All authors have read and agreed to the published version of the manuscript.

Funding: This research was funded by China Postdoctoral Science Foundation (Grant number 2020M681286).

Institutional Review Board Statement: Not applicable.

Informed Consent Statement: Not applicable.

Data Availability Statement: Not applicable.

Conflicts of Interest: The authors declare no conflict of interest.

References

1. Sha, D.; Bajic, V.B.; Yang, H. New model and sliding mode control of hydraulic elevator velocity tracking system. *Simulat. Pract. Theory* **2002**, *9*, 365–385. [CrossRef]
2. Yang, H.; Yang, J.; Xu, B. Computational simulation and experimental research on speed control of VVVF hydraulic elevator. *Control Eng. Pract.* **2004**, *12*, 563–568.
3. Nam, Y.; Hong, S.K. Force control system design for aerodynamic load simulator. *Control Eng. Pract.* **2002**, *10*, 549–558. [CrossRef]
4. Truong, D.Q.; Ahn, K.K. Force control for hydraulic load simulator using self-tuning grey predictor—Fuzzy PID. *Mechatronics* **2009**, *19*, 233–246. [CrossRef]
5. Sirouspour, M.R.; Salcudean, S.E. Nonlinear control of hydraulic robots. *IEEE Trans. Rob. Autom.* **2001**, *17*, 173–182. [CrossRef]
6. Zhu, W.-H.; Piedboeuf, J.-C. Adaptive Output Force Tracking Control of Hydraulic Cylinders with Applications to Robot Manipulators. *J. Dyn. Syst. Meas. Control* **2005**, *127*, 206. [CrossRef]
7. Guo, K.; Pan, Y.; Yu, H. Composite Learning Robot Control with Friction Compensation: A Neural Network-Based Approach. *IEEE Trans. Ind. Electron.* **2019**, *66*, 7841–7851. [CrossRef]
8. Guo, K.; Pan, Y.; Zheng, D.; Yu, H. Composite learning control of robotic systems: A least squares modulated approach. *Automatica* **2020**, *111*, 108612. [CrossRef]
9. Farivarnejad, H.; Moosavian, S.A.A. Multiple Impedance Control for object manipulation by a dual arm underwater vehicle–manipulator system. *Ocean. Eng.* **2014**, *89*, 82–98. [CrossRef]
10. Wang, T.; Li, Y.; Zhang, J.; Zhang, Y. A novel bilateral impedance controls for underwater tele-operation systems. *Appl. Soft Comput.* **2020**, *91*, 106194. [CrossRef]
11. Wang, Q.; Xie, X.; Shahrour, I.; Huang, Y. Use of deep learning, denoising technic and cross-correlation analysis for the prediction of the shield machine slurry pressure in mixed ground conditions. *Autom. Constr.* **2021**, *128*, 103741. [CrossRef]
12. Zhang, H.; Fang, J.; Yu, H.; Hu, H.; Yang, Y. Disturbance observer-based adaptive position control for a cutterhead anti-torque system. *PLoS ONE* **2022**, *17*, e0268897. [CrossRef] [PubMed]
13. Hogan, N. Impedance control: An approach to manipulation: Part I—Theory. *J. Dyn. Syst. Meas. Control* **1985**, *107*, 1–7. [CrossRef]
14. Hogan, N. Impedance control: An approach to manipulation: Part II—Implementation. *J. Dyn. Syst. Meas. Control* **1985**, *107*, 8–16. [CrossRef]
15. Hogan, N. Impedance Control: An Approach to Manipulation: Part III—Applications. *J. Dyn. Syst. Meas. Control* **1985**, *107*, 17–24. [CrossRef]
16. Jamwal, P.K.; Hussain, S.; Ghayesh, M.H.; Rogozina, S.V. Impedance Control of an Intrinsically Compliant Parallel Ankle Rehabilitation Robot. *IEEE Trans. Ind. Electron.* **2016**, *63*, 3638–3647. [CrossRef]
17. Hyun, D.J.; Seok, S.; Lee, J.; Kim, S. High speed trot-running: Implementation of a hierarchical controller using proprioceptive impedance control on the MIT Cheetah. *Int. J. Robot Res.* **2014**, *33*, 1417–1445. [CrossRef]
18. Zhang, J.; Liu, W.; Gao, L.E.; Li, L.; Li, Z. The master adaptive impedance control and slave adaptive neural network control in underwater manipulator uncertainty teleoperation. *Ocean. Eng.* **2018**, *165*, 465–479. [CrossRef]
19. Michel, Y.; Rahal, R.; Pacchierotti, C.; Giordano, P.R.; Lee, D. Bilateral Teleoperation With Adaptive Impedance Control for Contact Tasks. *IEEE Robot. Autom. Lett.* **2021**, *6*, 5429–5436. [CrossRef]
20. Hu, H.; Cao, J. Adaptive variable impedance control of dual-arm robots for slabstone installation. *ISA Trans.* **2022**, *128*, 397–408. [CrossRef]
21. Zhao, X.; Han, S.; Tao, B.; Yin, Z.; Ding, H. Model-Based Actor–Critic Learning of Robotic Impedance Control in Complex Interactive Environment. *IEEE Trans. Ind. Electron.* **2022**, *69*, 13225–13235. [CrossRef]
22. Plummer, A.R. Feedback linearization for acceleration control of electrohydraulic actuators. *Proc. Inst. Mech. Eng. Part I J. Syst. Contr. Eng.* **2005**, *211*, 395–406. [CrossRef]
23. Daher, N.; Ivantysynova, M. An Indirect Adaptive Velocity Controller for a Novel Steer-by-Wire System. *J. Dyn. Syst. Meas. Control. Trans. ASME* **2014**, *136*, 051012. [CrossRef]
24. Ahn, K.K.; Nam, D.N.C.; Jin, M. Adaptive Backstepping Control of an Electrohydraulic Actuator. *IEEE/ASME Trans. Mech.* **2014**, *19*, 987–995. [CrossRef]
25. Zhu, D. Sliding mode synchronous control for fixture clamps system driven by hydraulic servo systems. *Proc. Inst. Mech. Eng. C J. Mec.* **2007**, *221*, 1039–1045.
26. Lin, Y.; Shi, Y.; Burton, R. Modeling and robust discrete-time sliding-mode control design for a fluid power electrohydraulic actuator (EHA) system. *IEEE/ASME Trans. Mech.* **2013**, *18*, 1–10. [CrossRef]
27. Yao, B.; Tomizuka, M. Adaptive robust control of SISO nonlinear systems in a semi-strict feedback form. *Automatica* **1997**, *33*, 893–900. [CrossRef]
28. Yao, B.; Bu, F.P.; Reedy, J.; Chiu, G.T.C. Adaptive robust motion control of single-rod hydraulic actuators: Theory and experiments. *IEEE/ASME Trans. Mech.* **2000**, *5*, 79–91.
29. Chen, Z.; Yao, B.; Wang, Q.F. Accurate Motion Control of Linear Motors With Adaptive Robust Compensation of Nonlinear Electromagnetic Field Effect. *IEEE/ASME Trans. Mech.* **2013**, *18*, 1122–1129. [CrossRef]
30. Zhang, Q.; Fang, J.H.; Wei, J.H.; Xiong, Y.; Wang, G. Adaptive robust motion control of a fast forging hydraulic press considering the nonlinear uncertain accumulator model. *Proc. Inst. Mech. Eng. Part I J. Syst. Contr. Eng.* **2016**, *230*, 483–497. [CrossRef]

31. Chen, S.; Chen, Z.; Yao, B.; Zhu, X.; Zhu, S.; Wang, Q.; Song, Y. Adaptive robust cascade force control of 1-DOF hydraulic exoskeleton for human performance augmentation. *IEEE/ASME Trans. Mech.* **2017**, *22*, 589–600. [CrossRef]
32. Chen, W.H. Disturbance observer based control for nonlinear systems. *IEEE/ASME Trans. Mech.* **2004**, *9*, 706–710. [CrossRef]
33. Guo, K.; Wei, J.H.; Fang, J.H.; Feng, R.L.; Wang, X.C. Position tracking control of electro-hydraulic single-rod actuator based on an extended disturbance observer. *Mechatronics* **2015**, *27*, 47–56. [CrossRef]
34. Li, S.Z.; Wei, J.H.; Guo, K.; Zhu, W.L. Nonlinear Robust Prediction Control of Hybrid Active-Passive Heave Compensator with Extended Disturbance Observer. *IEEE Trans. Ind. Electron.* **2017**, *64*, 6684–6694. [CrossRef]
35. Wei, J.; Zhang, Q.; Li, M.; Shi, W. High-performance motion control of the hydraulic press based on an extended fuzzy disturbance observer. *Proc. Inst. Mech. Eng. Part I J. Syst. Contr. Eng.* **2016**, *230*, 1044–1061. [CrossRef]
36. Zhang, Q.; Wei, J.; Fang, J.; Li, M. Nonlinear motion control of the hydraulic press based on an extended piecewise disturbance observer. *Proc. Inst. Mech. Eng. Part I J. Syst. Contr. Eng.* **2016**, *230*, 830–850. [CrossRef]
37. Shi, W.; Wei, J.; Fang, J.; Li, M. Nonlinear cascade control of high-response proportional solenoid valve based on an extended disturbance observer. *Proc. Inst. Mech. Eng. Part I J. Syst. Contr. Eng.* **2018**, *233*, 921–934. [CrossRef]
38. Li, M.; Shi, W.; Wei, J.; Fang, J.; Guo, K.; Zhang, Q. Parallel Velocity Control of an Electro-Hydraulic Actuator with Dual Disturbance Observers. *IEEE Access* **2019**, *7*, 56631–56641. [CrossRef]
39. Wang, L.-X. *A Course in Fuzzy Systems and Control*; Prentice Hall: Englewood Cliffs, NJ, USA, 1996.
40. Ho, T.H.; Ahn, K.K. Speed control of a hydraulic pressure coupling drive using an adaptive fuzzy sliding-mode control. *IEEE/ASME Trans. Mech.* **2012**, *17*, 976–986. [CrossRef]
41. Tian, Q.Y.; Wei, J.H.; Fang, J.H.; Guo, K. Adaptive fuzzy integral sliding mode velocity control for the cutting system of a trench cutter. *Front. Inform. Technol. Electron. Eng.* **2016**, *17*, 55–66. [CrossRef]
42. Shibata, M.; Murakami, T.; Ohnishi, K. A unified approach to position and force control by fuzzy logic. *IEEE Trans. Ind. Electron.* **1996**, *43*, 81–87. [CrossRef]
43. Xu, Z.-L.; Fang, G. Fuzzy-Neural Impedance Control for Robots. In *Robotic Welding, Intelligence and Automation*; Tarn, T.-J., Zhou, C., Chen, S.-B., Eds.; Springer: Berlin/Heidelberg, Germany, 2004; pp. 263–275.
44. Fateh, M.M.; Alavi, S.S. Impedance control of an active suspension system. *Mechatronics* **2009**, *19*, 134–140. [CrossRef]
45. Yao, B.; Bu, F.P.; Chiu, G.T.C. Non-linear adaptive robust control of electro-hydraulic systems driven by double-rod actuators. *Int. J. Control* **2001**, *74*, 761–775. [CrossRef]
46. Xu, Q. Robust impedance control of a compliant microgripper for high-speed position/force regulation. *IEEE Trans. Ind. Electron.* **2015**, *62*, 1201–1209. [CrossRef]
47. Slotine, J.-J.E.; Li, W. *Applied Nonlinear Control*; Prentice Hall: Englewood Cliffs, NJ, USA, 1991.